


2013

CO-ELECTROPHORETIC DEPOSITION OF LIQUID METAL AND SILICON FOR LITHIUM-ION BATTERY APPLICATION

Hanfei Zhang
Michigan Technological University


Follow this and additional works at: <https://digitalcommons.mtu.edu/etds>

 Part of the [Energy Systems Commons](#), and the [Nanoscience and Nanotechnology Commons](#)
Copyright 2013 Hanfei Zhang

Recommended Citation

Zhang, Hanfei, "CO-ELECTROPHORETIC DEPOSITION OF LIQUID METAL AND SILICON FOR LITHIUM-ION BATTERY APPLICATION", Master's Thesis, Michigan Technological University, 2013.
<https://doi.org/10.37099/mtu.dc.etds/655>

Follow this and additional works at: <https://digitalcommons.mtu.edu/etds>

 Part of the [Energy Systems Commons](#), and the [Nanoscience and Nanotechnology Commons](#)

CO-ELECTROPHORETIC DEPOSITION OF LIQUID METAL AND
SILICON FOR LITHIUM-ION BATTERY APPLICATION

By

Hanfei Zhang

A THESIS

Submitted in partial fulfillment of the requirements for the degree of

MASTER OF SCIENCE

In Mechanical Engineering

MICHIGAN TECHNOLOGICAL UNIVERSITY

2013

© 2013 Hanfei Zhang

This thesis has been approved in partial fulfillment of the requirements for the Degree of MASTER OF SCIENCE in Mechanical Engineering

Department of Mechanical Engineering - Engineering Mechanics

Thesis Advisor: *Dennis Desheng Meng*

Committee Member: *Craig Friedrich*

Committee Member: *Yun Hang Hu*

Committee Member: *Kazuya Tajiri*

Department Chair: *William W. Predebon*

Table of Content

Table of Content	3
Acknowledgements	5
Abstract	5
1. Introduction	6
1.1. Lithium-ion battery (LIB)	6
1.1.1. Current status and issue	7
1.1.2. Si based negative electrode.....	8
2. Goals and hypotheses	9
2.1. Gallium / Galinstan on LIBs application	10
2.2. Electrophoretic deposition of liquid metal.....	11
3. Methods	13
3.1. EPD of gallium.....	13
3.1.1. Stability of dispersion	14
3.1.2. Gallium deposition.....	17
3.1.3. Gallium patterns.....	18
3.2. Co-EPD of silicon and gallium / galinstan	20

3.3.	LIBs half-cell testing.....	21
4.	Results	21
4.1.	EPD of Gallium.....	21
4.1.1.	Charging salt	24
4.1.2.	High deposition rate.....	26
4.1.3.	Scalability	27
4.2.	Si-Galinstan co-EPD	29
4.3.	LIBs half-cell testing result.....	30
5.	Discussion	32
5.1.	Analysis of co-EPD parameters	32
5.2.	Core-shell structure obtained by co-EPD	35
5.3.	Half-cell test performance.....	37
5.4.	Issues and challenges – Ga-Li system	39
6.	Future Work.....	41
6.1.	Application of liquid metal thin film by EPD - CIGS solar cell	41
7.	Conclusion	42
	Reference	43

Acknowledgements

Author acknowledges the support from Dr. Dennis Desheng Meng, MuSES lab members: Sunand Santhanagopalan, Anirudh Balram, Xiaobao Geng, Bryan Steinhoff, Ryan Lemmens and alumni lab member Yiping Feng. Author also acknowledges the support on lithium-ion battery half-cell testing conducted by Dr. Yan Yao and Dr. Leonard Liang from University of Houston.

Abstract

A low cost electrophoretic deposition (EPD) process was successfully used for liquid metal thin film deposition with a high depositing rate of 0.6 $\mu\text{m}/\text{min}$. Furthermore, silicon nano-powder and liquid metal were then simultaneously deposited as the negative electrode of lithium-ion battery by a technology called co-EPD. The liquid metal was hoping to act as the matrix for silicon particles during lithium ion insertion and distraction. Half-cell testing was performed using as prepared co-EPD sample. An initial discharge capacity of 1500 mAh/g was reported for nano-silicon and galinstan electrode, although the capacity fading issue of these samples was also observed.

1. Introduction

1.1. Lithium-ion battery (LIB)

Using lithium-ion batteries for energy storage has been widely accepted by manufacturers of cell phone, laptop computer and electric vehicle. The main advantage of lithium-ion chemistry is that it has a relevantly high energy density for battery application; the problem is it is not high enough, especially for electric vehicle applications, although its safety has always been pointed out as an issue.

Lithium-ion batteries transfer the electric energy through the insertion and extraction process of lithium ion between two electrodes. During discharge (*Fig.1.1*), because of the chemistry potential difference, lithium ions tend to leave negative electrode material (i.e. graphite) and travel to join the positive electrode material (i.e. CoO_2 or FePO_4). At the same time, the electrons emigrating from negative electrode to positive electrode through an outer loop are utilized to generate electric power.

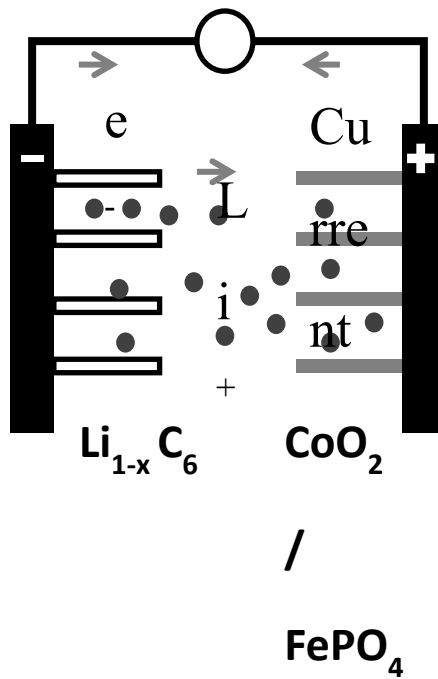


Fig.1.1 Schematic working mechanism of lithium-ion chemistry

1.1.1. Current status and issue

As shown in *Fig.1.1*, the capacity of the cell is decided by the quantity of electron-lithium ion pairs that are able to be transferred between the two electrodes. This capacity is based upon the insertion of the lithium ions into the active material and is dependent on the chemical structure of the compounds. Graphite is the most popular negative active material for commercialized lithium-ion batteries, and the theoretical capacity of the graphite electrode (LiC_6) is 372 mAh/g [1]. Much work has been done to improve the capacity of carbon based lithium-ion batteries, such

as using carbon nanotubes (CNTs) [2]. However, since the energy density for current negative electrode materials are still not enough, it is time to look for alternative active materials for lithium-ion batteries.

1.1.2. Si based negative electrode

Among all the current materials been tested, the formation of the compound of $\text{Li}_{4.4}\text{Si}$ with lithium, silicon as a negative electrode material has the highest theoretical insertion capacity of 4200 mAh/g [3]. However, the major issue with silicon in this application is the huge volume change during insertion and extraction of the lithium (300%) which can cause silicon breakdown and cause contact loss with the substrate [4]. This is why a fast capacity fade was observed for Si based lithium-ion batteries.

Many works have been done to solve this problem. Aifantis, et.al was trying to explain and model the crack formation by using a previously developed formula and Rongguan Lv, et al. electrodeposited porous Si-Li system to buffer the breakdown, a 90% capacity remains after first charge-discharge cycle [5, 6]. Additionally, Yi Cui, et.al has been synthesizing Si nanostructures such as Si nanowires and Si nanotubes for this application. By taking advantage of these nanostructures, the

theoretical capacity (4200 mAh/g) was observed and the capacity is maintained around 3000 mAh/g for more than 200 charge-discharge cycles [7, 8]. Another effort was made by Liwen Ji, et.al were a graphene and Si multiple layers structure with the intention of using graphene as the matrix to buffer the volume increasing of Si during insertion [9]. All these efforts have been made to find a way to buffer the breakdown of the silicon and to increase the conductivity between the active material and the current collector.

2. Goals and hypotheses

This work is aimed to fabricate a silicon based negative electrode with an accompanying matrix around the silicon particles. This matrix material should be able to compensate for volume change of the silicon during the lithium insertion and furthermore, it also should be able to act as a conductive bridge between the Si particles and the current collector after breakdown. Liquid metal was considered as the matrix since it can satisfy both requirements; the expansion of silicon particles during insertion is expected to be compensated by the liquid property of the metal while the active material will be kept conductive after breakdown - because the conductive liquid metal will fill into the cracks. The whole

idea is illustrated in *Fig.2.1*

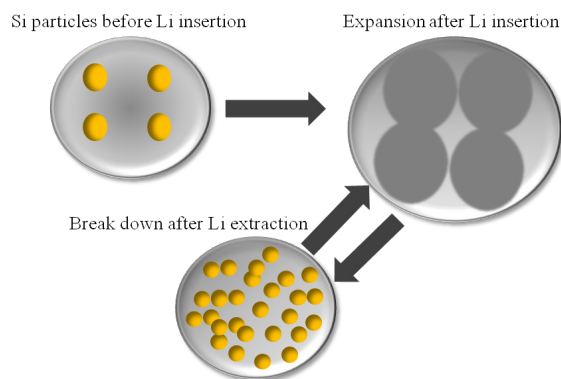


Fig.2.1 Schematic explanation of using liquid metal as the matrix for silicon based negative electrode for lithium-ion batteries

2.1. Gallium / Galinstan on LIBs application

Gallium and its compounds can find many applications in microelectronics, solar cells, microwave circuitry and optoelectronic devices [10-14]. With the melting point of 29.8°C, gallium can be the liquid matrix at the operational status of Si based lithium-ion batteries. Galinstan is a eutectic alloy of gallium (typical 68w%), indium (typical 22w%) and tin (typical 10w%) with a melting point even lower than that of each individual element. The melting point of galinstan is typically 19°C which implies that the alloy will be a liquid at any phase of

lithium-ion battery operation.

2.2. Electrophoretic deposition of liquid metal

Mixing silicon and liquid metal is difficult. This is because liquid metal doesn't wet silicon. Several methods including mechanical agitating, high voltage deposition of silicon into gallium electrode and pasting were explored by a previous M.S. student (Yiping Feng). Unfortunately, a well distributed mixture with high silicon content was not obtained.

Electrophoretic deposition (EPD) is known for its low cost, versatility, and excellent scalability [15]. The deposition relies on the net charge on the surface of solid particles dispersed in a liquid medium due to the formation of electric double layers (EDLs). As illustrated in *Fig.2.2*, when dispersed in the solution, self-negatively charged particle attracts the oppositely charged ions and molecules via the electrostatic force. The first layer formed around the particle is immobilized and called 'Stein Layer'. Outside of the stein plane, some charged particles in the surrounding form a loosely attached 'diffusion layer'. The boundary between the diffusion layer and the bulk solution is called 'Slipping Plane'. In this double layer system, stein plane has the highest potential, and it decreases to near 0 at a distance far away from the stein plane. The

potential on the slipping plane is called ‘Zeta Potential’, which is a crucial indicator of how strong the double layer system reacts to an applied electric field.

When subjected to an electric field, the charged solid particles, now are actually EDL systems, can be moved to the oppositely-charged electrode and get deposited. The deposition rate is thus independent of the electrochemical potential of the species being deposit, potentially easing the composition control of co-deposition.

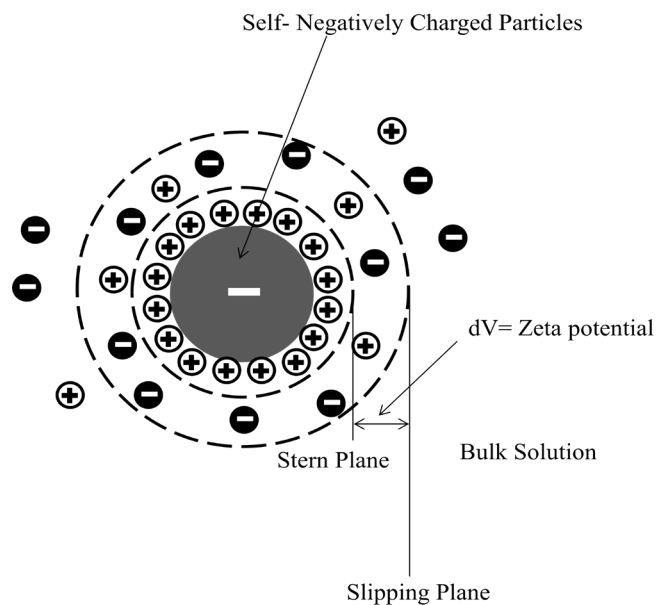


Fig.2.2 Schematic view of the electrical double layer system

Based on the author’s knowledge, EPD of liquid metal has yet been

reported by any organization or personnel. But based on the mechanism of EPD, it has the potential to deposit any type of metal droplets if they have enough electrical charges on their surfaces. Furthermore, it may be possible to deposit multiple elements in one step by using the electrophoresis mechanism if the droplets have enough electrical charge on them.

This work is to present a low cost, one-step electrophoresis method to fabricate a silicon thin film with the liquid metal around it as the matrix, and to use it as the negative electrode of a lithium-ion battery.

3. Methods

3.1. EPD of gallium

Gallium (Alfa Aesar, 99.9% purity) is first dispersed in isopropyl alcohol (IPA) (Pharmco-AAPER, 99% purity) at a concentration of 0.5 mg/ml by sonication at a power of 130W for 25 minutes with an ultrasonic processor (Sonics & Materials Inc., VCX130). In order to keep the dispersion stable and facilitate EPD, magnesium nitrate hexahydrate

(Fisher Scientific, 99% purity) is also added to charge the gallium droplets. Since gallium tends to form alloy with many metals, the materials for handling tools and containers are carefully chosen, such as polyethylene [16]. At the same time, gallium is kept in IPA whenever possible (e.g., during weighing) to avoid oxidation.

3.1.1. Stability of dispersion

A stable colloid dispersion is normally believed as a requirement for successful EPD. However, according to Joung, et al, EPD is also possible with an unstable dispersion, but the surface of the deposited film is rough [17]. This is because the particles in an unstable dispersion tend to coagulate with each others during EPD process. *Fig.3.1* schematically demonstrates the difference between EPD of a colloid and an unstable dispersion. Colloid contains well-distributed particles with similar electric charge density, which is mainly depends on the zeta potential. On the other hand, the colloid becomes unstable if the charge density on the particles are not high enough to keep particles from coagulation. As a result, EPD on an unstable dispersion will result in clump formation of the deposited film. Due to the importance of well-mixing of two materials, clumps formation needs to be avoid in this

case, so the stability of the dispersion was first observed.

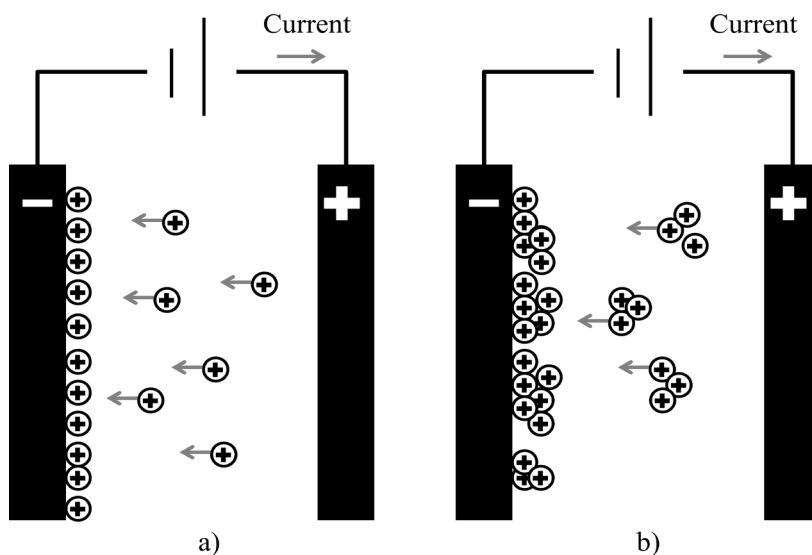


Fig.3.1. Electrophoretic deposition (EPD) on a) a stable dispersion and b) an unstable dispersion

Gallium, as a metal with low melting point (29.9°C), forms liquid droplets in the dispersion after sonication as a result of ultrasonic heating, e.g., the dispersion normally reaches a temperature of $\sim 50^{\circ}\text{C}$ right after sonication. Unlike solid particles, the gallium droplets can easily coagulate with each other shortly after the sonication. Such a colloid of gallium at room temperature completely collapses within a few hours as evidenced by the precipitate observed on the bottom of the testing tube (**Fig. 3.2a**) and the clear liquid seen at the side (**Fig. 3.2c**) after 2 hours. In this work, the stability of the dispersion is improved by quenching the

dispersion to a lower temperature so that the gallium can be solidified while the viscosity of IPA being increased [18]. The quenching is achieved by directly adding dry ice into the dispersion right after sonication. By doing this, the temperature of the dispersion is brought down to about -30°C within 1 minute. The dispersion is sonicated again by an ultrasonic cleaner (Branson Ultrasonics Corporation, Bransonic 1510) at a power of 70W for a few minutes in order to remove the carbon dioxide dissolved in the dispersion and further stabilize it. Then the dispersion is stored at -15°C for stability characterization. No significant precipitate has been observed on the bottom of the testing tube after 2 hours (*Fig. 3.2b*) while the side view still remains cloudy (*Fig. 3.2d*). The observation indicates improved stability of at least 2 hours at -15°C , which is later proved to be sufficient for successful EPD. The dispersion has also been stored in a freezer (Kendro Laboratory Products, Isotemp Basic) at about -75°C , where it can be stable for about 3 days. Our observation on improved dispersion stability at low temperature agrees with previous reports on obtaining stable gallium-organic solvent dispersions by co-condensation at low temperature (e.g., 77K), where IPA was identified as the preferable solvent for high stability [19].

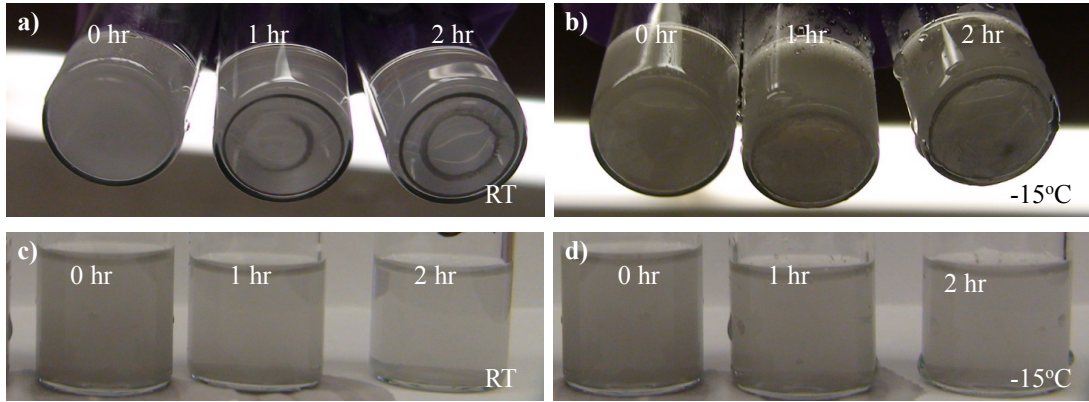


Fig.3.2 *Stability of gallium-IPA dispersion before (a&c, labeled as RT for room temperature) and after (b&d) quenching by dry ice. Each picture shows the status of 3 samples at 0 hour, 1 hour or 2 hours after sonication. The stability can be judged by whether precipitate is formed on the bottom (a&b) and whether the side view turns clear (c&d).*

3.1.2. Gallium deposition

With a stable dispersion, EPD is performed at -15°C in a salt ice bath with two stainless steel plates (25mm x 19mm x 2mm) as the electrodes [20]. An electric field of 600 V/cm is supplied by a high voltage power source (Stanford Research System Inc., Model PS 325/2500 V-25W). The charging agent, magnesium nitrate hexahydrate, is also co-deposited as magnesium compounds (see next section for details), which can be removed by weak acetic acid after EPD. The deposited samples were

observed under a field emission scanning electron microscope (FESEM) with energy dispersed spectroscopy (EDS) capability (Hitachi, Hitachi 6400). The particle size was analyzed by software ImageJ (National Institute of Health) from the FESEM pictures. The weight of the deposit is measured by a high-precision (0.1 mg resolution) analytical balance (Adam Equipment Inc., PW124 Lab Balance) and the thickness of the deposits is measured by a laser profile scanner (Optical Gaging Products, Cobra).

3.1.3. Gallium patterns

As previously mentioned, gallium compounds like gallium arsenide and gallium nitride can find many applications in electronic and optical devices. The EPD method reported herein can potentially offer a low-cost, scalable alternative to chemical vapor deposition (CVD) and other existing processes. In order to verify its compatibility with microfabrication, several gallium micro patterns were obtained by masking the substrate during EPD. A cutter (Silhouette American Inc., Silhouette CAMEO) was used to pattern adhesive-loaded vinyl tapes (Silhouette American Inc.) as the masks. In particular, gallium micropatterns with feature size ranging from 300 μm (*Fig. 3.3a*) to 2mm

(*Fig. 3.3c*) were formed on the stainless steel substrates. The vinyl tape mask is carefully removed after deposition, followed by rinsing the samples by acetone carefully to remove the residue of adhesive. Finally, the binder (Mg compounds) could be removed by diluted acetic acid if needed.

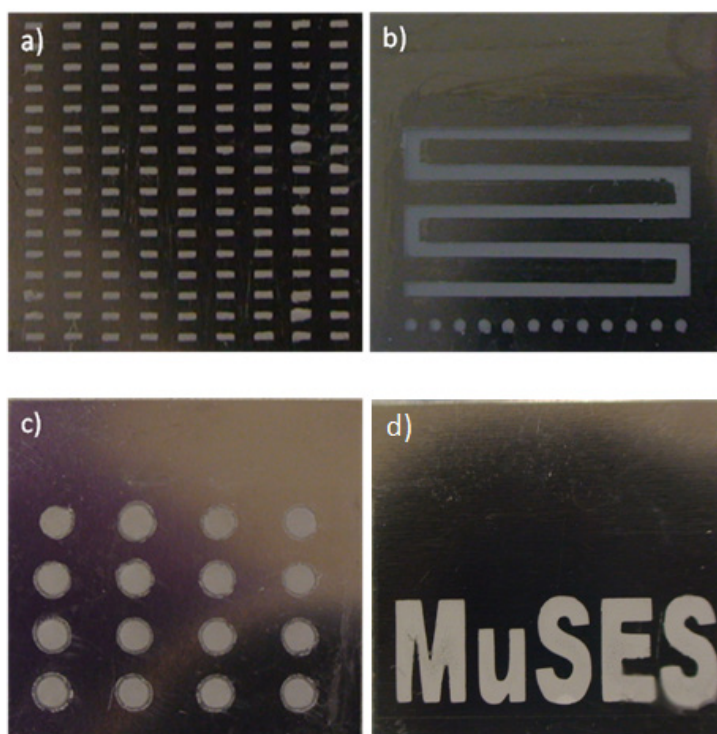


Fig.3.3: Variable patterns of gallium on stainless steel substrate. a) 1mm x 300 μ m rectangular arrays; b) 1 mm diameter circles & 1 mm width lines; c) circles of 2 mm in diameter; d) pattern of letters.

3.2. Co-EPD of silicon and gallium / galinstan

Silicon nano-powder (Meliorum Technologies, 5 nm) and silicon micron-powder (Alfa Aesar, 1-5 micron, 99.9% purity) were dispersed in IPA by using the ultrasonic cleaner. Gallium and galinstan (Roto Metals) dispersions were prepared exactly by the method presented in section 3.1 since galinstan is acting similarly to gallium in this process. $\text{Mg}(\text{ON})_2$ was first used as the charging salt, but unfortunately, the non-conductive holding layer formed by Mg^{2+} ions was found to weaken the battery cell performance testing. To solve this problem, an alternative salt, $\text{NiCl}_2 \cdot 6\text{H}_2\text{O}$ (J.T.Baker[®] BAKER ANALYZED[™] reagent) was used as a conductive binder [21]. The concentration of charging salt was kept the same (0.03 mg/ml) for both the silicon dispersion as well as the liquid metal dispersion.

The silicon dispersion and liquid metal dispersion were mixed in a new container at different ratios (Si : liquid metal (mg/ml) = 1:5, 1:3, 1:2, 1:1 and 2:1) as the precursors of co-EPD dispersion. These precursors dispersion were then sonicated again in the ultrasonic cleaner. Masked copper foil (Mcmaster, 0.5 mm thick) and stainless steel were used as the negative and positive electrode respectively. Finally, EPD was

performed with an electric field of 600V/cm.

3.3. LIBs half-cell testing

Nano-silicon and micron-silicon powder were co-deposited with galinstan respectively on a masked copper substrate as the electrode of lithium-ion battery. The as deposited samples were carefully packaged and sent to university of Houston for lithium-ion coin cell assembly and charge/discharge cycling testing. The cell was made and tested at a rate of C/20 by Leonard Liang and Yan Yao from university of Houston. 1 M LiClO₄ in ethylene carbonate (EC) / diethyl carbonate (DEC) (v/v=1/1) was used as the electrolyte. Double polymer was used as the separator.

4. Results

4.1. EPD of Gallium

After EPD, deposition was found on negative electrode which indicates that gallium particles are charged positively by Mg²⁺ ions. The deposited film is translucent with rainbow-colored reflection and near-spherical

gallium particles can be observed under FESEM as *Fig. 5a-c* show. During EPD, the charging salt $\text{Mg}(\text{NO}_3)_2$ is co-deposited to form $\text{Mg}(\text{OH})_2$ and $\text{Mg}(\text{C}_3\text{H}_7\text{O})_2$, which can serve as binder or holding layer, and are nonconductive, rendering them whitish color under FESEM [21, 22]. Additionally, the droplet particles still appear to be slightly whitish even after removing Mg compounds, which can be attributed to the oxidation of gallium. When the electron beam is focused on a particular particle for longer periods of time, melting and crack formation on the particle was observed (*Fig.4.1b*). To improve conductivity and remove impurities, the samples were carefully rinsed by weak acetic acid. *Fig.4.1c* shows the Energy-dispersive X-ray spectroscopy (EDS) data with a major peak of gallium and smaller peaks of magnesium and oxygen from the co-deposited compounds. By analyzing FESEM images with ImageJ, the average particle size was determined to be 727 ± 408 nm with the high deviation is a result of coagulation of gallium nano-droplets at high temperature during FESEM imaging.

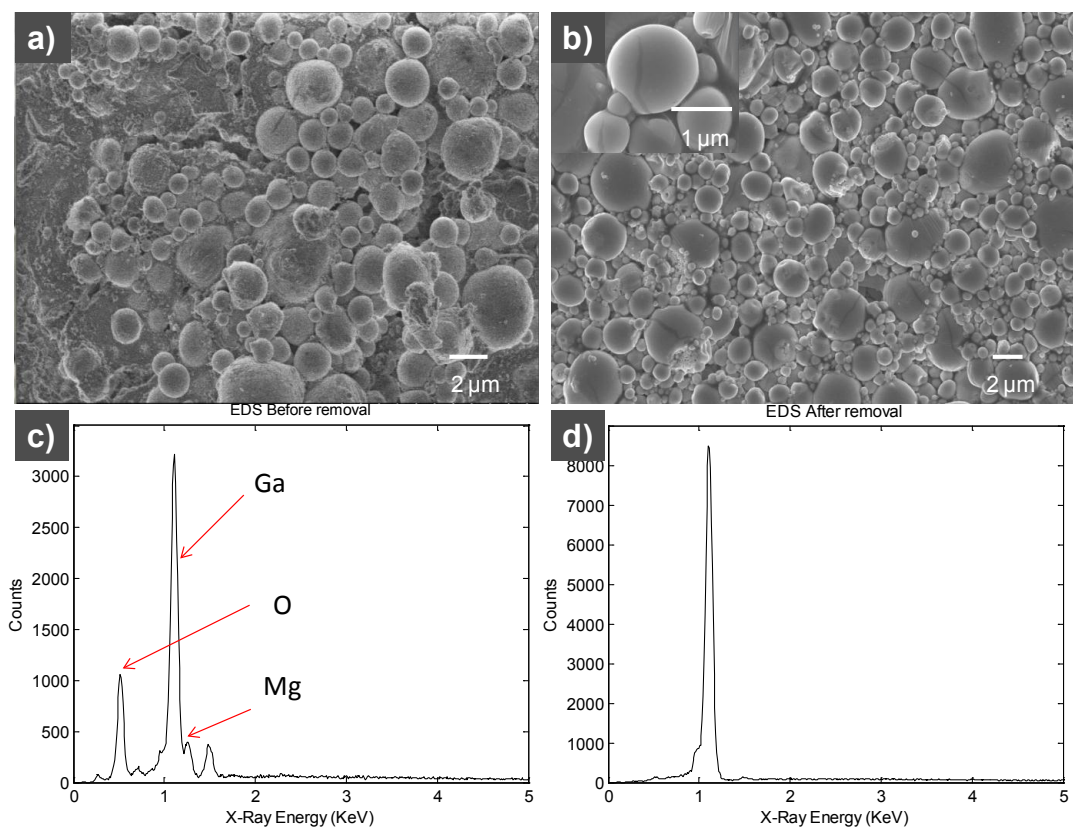


Fig.4.1: SEM and EDS of the deposit. a) gallium particles with magnesium compounds holding layer; b) gallium particles after the removal of magnesium compounds and a zoon-in view on a few particles showing crack and passive oxide layer; c);EDS of the film before removal of magnesium compounds d) EDS of the film after removal of magnesium compounds;.

4.1.1. Charging salt

The concentration of Mg^{2+} , the charging agent, plays a critical role on the deposition rate and the film quality. To get reliable, high-quality depositions, the Mg^{2+} ions should be enough to charge the gallium particles yet not too high to avoid excessive ionic strength which thins the electric double layer [15]. Meanwhile, high concentration of Mg^{2+} may result in the quick formation of a low-conductive layer, leading to a slower deposition rate. However, this factor is not explicitly included in classic Hamaker's law for EPD and thus deemed worthy to be determined experimentally [23].

To define the optimal concentration of magnesium nitrate, $C[Mg(NO_3)_2]$, EPD at different values was performed while other key parameters such like electric field, temperature and deposition time are kept constant. The result is shown in **Fig.4.2**. The yield of gallium reaches a peak at $C[Mg(NO_3)_2]=0.05$ mg/ml although the yield of the magnesium compounds is almost the same for different concentrations (~ 0.14 mg/cm²). The experimental results have confirmed the aforementioned hypothesis of an optimal $C[Mg(NO_3)_2]$ value. It is also implied that the yield variation of the gallium is dominated by the EPD

as the result of tuning the amount of the charging salt instead of electrodeposition of magnesium compounds.

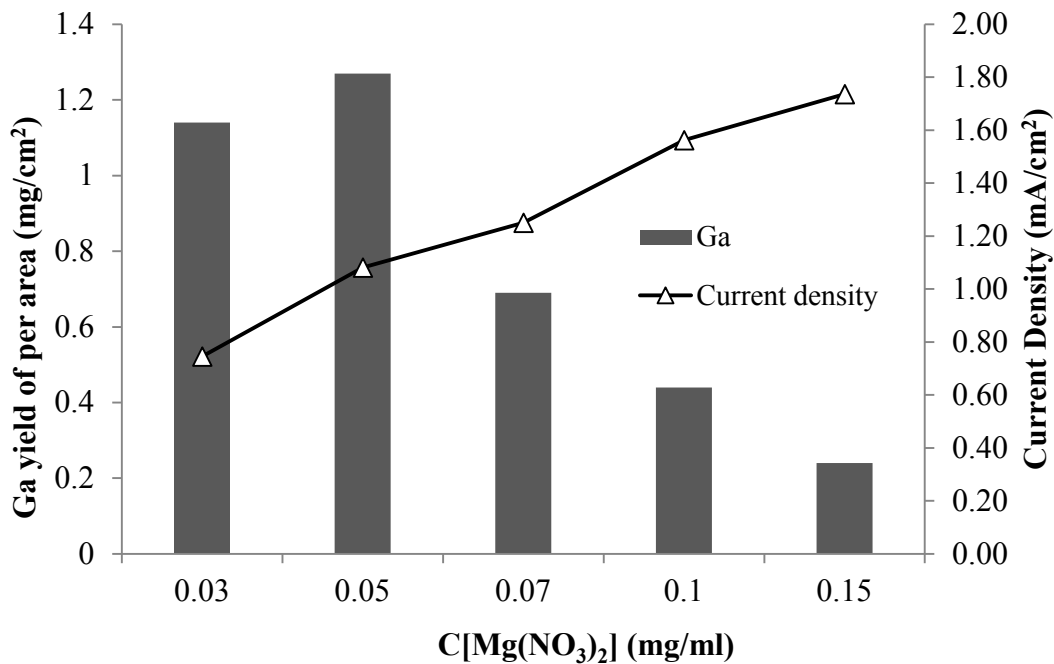


Fig.4.2: The deposition yield of different concentration of $Mg(NO_3)_2$.
Electric field strength: 600 v/cm; Concentration of gallium: 0.5 mg/ml;
Temperature: $-15\text{ }^\circ\text{C}$; Deposition time: 4 minutes

On the other hand, the average current density recorded in **Fig.4.2** during the EPD almost linearly depends on $C[Mg(NO_3)_2]$, reflecting the increasing conductivity of the dispersion .

4.1.2. High deposition rate

As mentioned above, a gallium yield of 1.27 mg/cm² (**Fig.4.2**) is obtained in 4 minutes' deposition for this specific experiment with C[Mg(NO₃)] = 0.05 mg/ml. In order to compare to the reported deposition rate of electroplating of gallium, which is around 2 μm per 30 min, the thickness of the electrophoretic deposited film is theoretically calculated and experimentally measured [24].

The theoretical deposition rate of 0.5 μm/min is first calculated by **eqn.4.1** by using the density of gallium (5.91 g/cm³).

$$Thickness = \frac{Mass(g)}{Density(g/cm^3) \cdot ElectrodeArea(cm^2)} \quad \text{eqn.4.1}$$

Then the thickness of this film with 8 minutes deposition is directly measured (Optical Gaging Products, Cobra) with a result of ~0.6 μm/min. This result concurs with the theoretical calculation and is almost an order of magnitude higher than the deposition rate of electroplating (~0.07 μm/min).

4.1.3. Scalability

In order to verify the scalability of the process, continuous deposition was performed and the yield was studied as a function of deposition time. The deposition time was divided into multiple steps, which each time step indicating 4 minutes of deposition, as shown in *Fig. 4.3*.

The deposition was carried out without removing the non-conductive holding layer ($\text{Mg}(\text{OH})_2$ and $\text{Mg}(\text{C}_3\text{H}_7\text{O})_2$) between the deposition steps. The obtained thin film on the stainless steel plate substrate was weighted (Adam Equipment Inc., PW124 Lab Balance) right after each deposition to determine the yield, which included the weight of Mg compound as binders. The concentration of the magnesium nitrite in the dispersion was 0.05 mg/ml, which has been verified previously as the optimal EPD parameters in this particular experiment. The electrical field strength and temperature were kept as 600 V/cm and -15°C respectively and from this, a fairly constant deposition rate is observed during this process. A film with yield of 6.9 mg/cm^2 ($\sim 12 \mu\text{m}$) is obtained after 24 minutes. By replenishing the dispersion for every 12 minutes, the yield after 24 minutes is only 6.9 % of the total gallium available in the dispersion, indicating the result of this test was not disturbed by the potential

decreasing of gallium concentration in the dispersion.

Additionally, a rapid decreasing of deposition rate was not observed during the experiment, which indicates this EPD process is compatible with continuous deposition even without the removal nonconductive holding layer.

It was also noticed that removal of the non-conductive binder by weak acid between each two deposition steps can lead to a higher gallium yield in this experiment. However, the rinse process should be performed carefully, otherwise the removal of the binder will make the deposited material falling off the substrate.

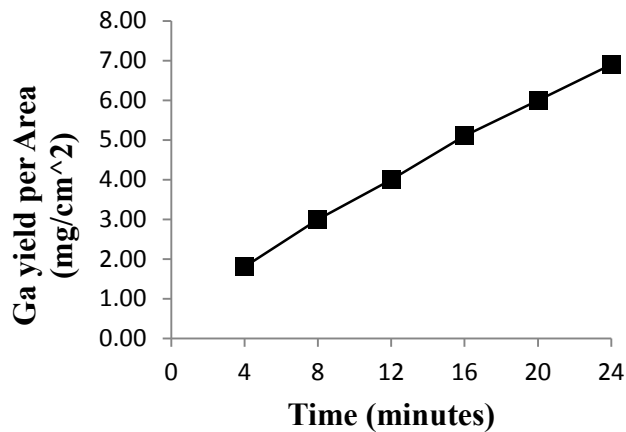


Fig.4.3: The deposition yield as a function of time. Electric field strength: 600 v/cm; concentration of $Mg(NO_3)_2$: 0.05 mg/ml; Concentration of gallium: 0.5 mg/ml; Temperature: $-15\text{ }^\circ\text{C}$.

4.2. Si-Galinstan co-EPD

Silicon and liquid metal co-EPD films were looked under FESEM and the quantitative weight percentages of the elements in the films were analyzed by EDS. **Fig.4.4** shows the FESEM image and EDS analysis of silicon and galinstan co-deposition. It is noticed that both nano-silicon powder and micron-silicon powder can be co-deposited with galinstan. However, by having the same concentration ratios of silicon and galinstan content in the dispersion, the weight percentage of each element in the yielded film is quite different due to the different silicon particle size. In order to show this phenomenon, an experiment regarding the yield percentage of the film as a function of the concentration ratio in the dispersion was conducted. The result will be discussed in next section of this work.

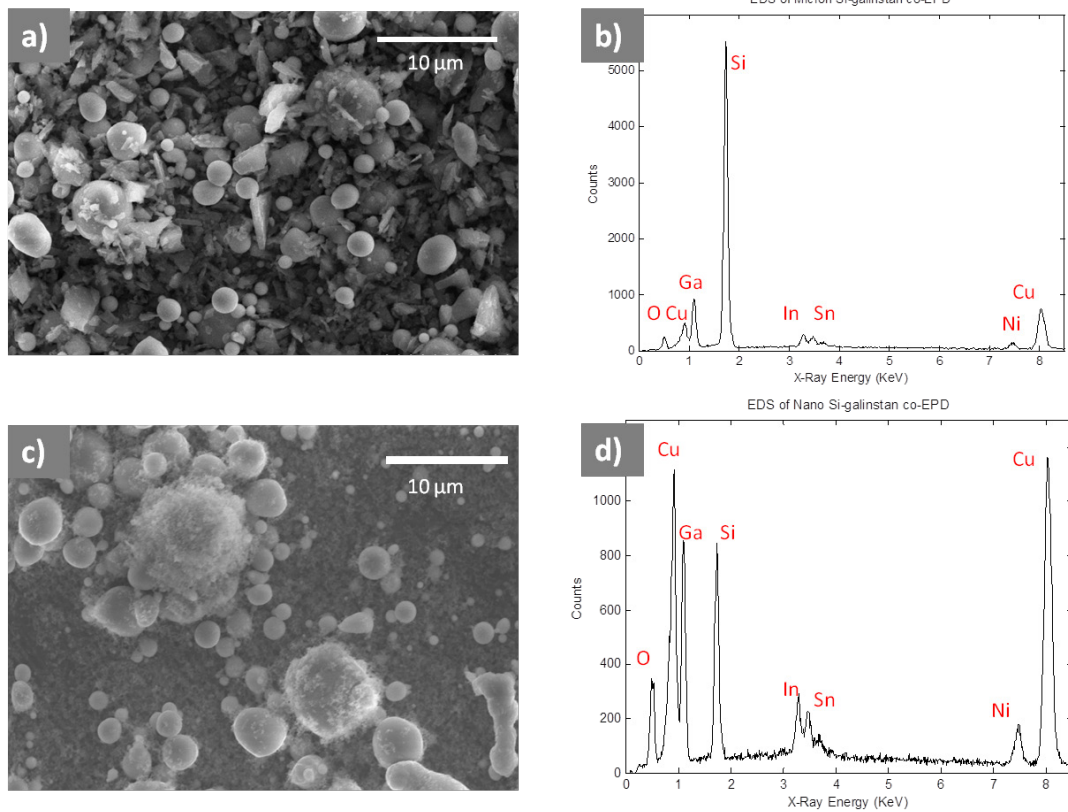


Fig.4.4 The FESEM image and EDS analysis of micron Si-galinstan co-EPD (a,b) and FESEM image and EDS analysis of nano Si-galinstan (c,d)

4.3. LIBs half-cell testing result

A first discharge capacity of 1500 mAh/g was got from a nano-silicon and galinstan sample ($\text{Si}_w\%=54\%$), however, a capacity fade was observed and only a capacity of 400 mAh/g remained after 3 cycles.

Most of the micron-silicon and galinstan samples have a much lower first discharge capacity of 100 - 300 mAh/g, with a ~50 mAh/g capacity after few cycles. This is shown in **Fig.4.5**.

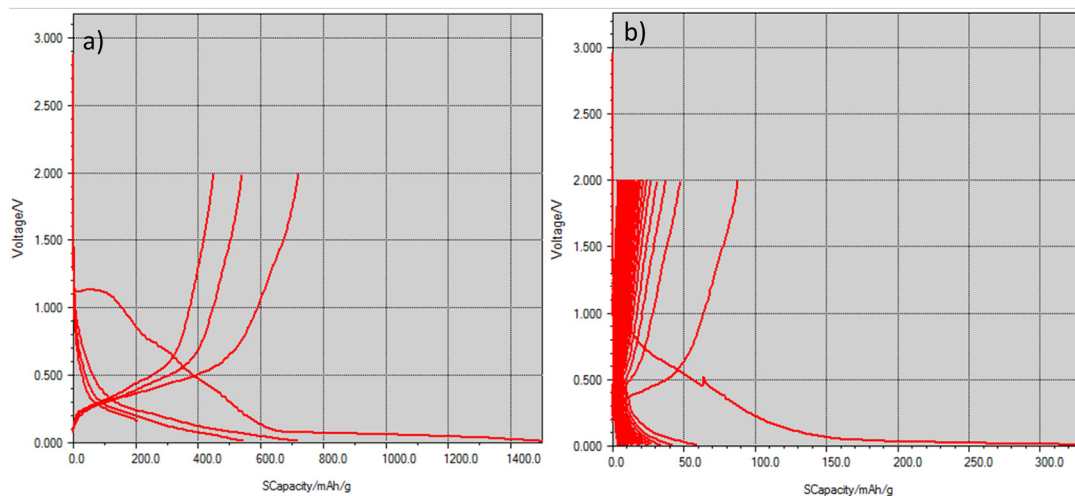


Fig.4.5 Half-cell test results a) Nano-Si sample with a 1st discharge capacity of 1500 mAh/g and b) micron-Si sample with a 1st discharge capacity of 300 mAh/g

5. Discussion

5.1. Analysis of co-EPD parameters

The yield percentage of each element during co-EPD was dependent on many parameters. Since this area has not been previously explored, the concentration and the particle size of each element in the dispersion, which are both believed to have a direct impact on the yield percentage, was experimentally verified by EDS.

In *Fig.5.1*, weight percentage of micron-silicon powder (solid line) and nano-silicon powder (dot line) after co-EPD are plotted as the function of the concentration ratio between silicon and galinstan in the dispersion. The deposition time, electric potential used, and the temperature were kept the same for every data points. It can be noted that with the higher silicon concentration in the dispersion, the silicon content in the yield is generally higher. However, there is also a silicon yield difference between nano-sized silicon and micron-sized silicon even at the same concentration ratio. Furthermore, unlike the micron-silicon curve which is 'smooth', the nano-silicon weight percentage is increasing with a

substantial increase between the concentration ratios of 0.3 to 0.5. After multiple tests it was seen that there is very little nano-silicon content for the concentration ratio lower than 0.3 (i.e. $C[\text{silicon}] = 0.3 \text{ mg/ml}$, $C[\text{galinstan}] = 1 \text{ mg/ml}$). In general, the yield for nano-sized silicon was lower than that of micron-sized silicon in this test.

This phenomenon may be explained by the different particle size of the two elements in the co-EPD dispersion. When the size of the particles and droplets are similar, for example micron-silicon powder (1-5 μm) and galinstan droplets ($\sim 1\text{-}10 \mu\text{m}$), the yield percentage of each element is more dependent on their concentrations in the co-EPD dispersion; on the other hand, if the size of the particles and droplets are orders of magnitude different, as is the case for the nano-silicon powder (5 nm) and galinstan droplets ($\sim 1\text{-}10 \mu\text{m}$), the yield cannot be easily related to the concentration ratio in the dispersion. Although the interaction between the silicon nano-particles and the galinstan micro-droplets during co-EPD is not fully understood, it is believed that there is a concentration threshold between 0.3 and 0.5 that the deposition of galinstan will be preferred.

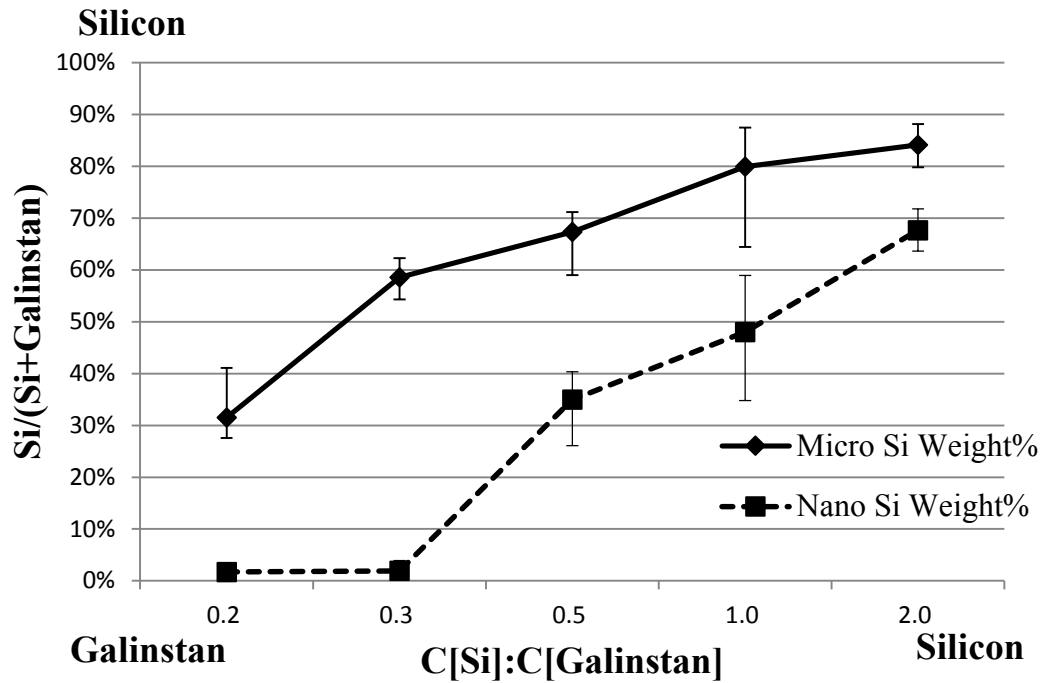


Fig.5.1 The silicon percentage after co-EPD as a function of concentration ratio in the dispersion. X-axis is the concentration ratio between silicon and galinstan in the dispersion; Y-axis is the silicon weight percentage in the film after deposition.

5.2. Core-shell structure obtained by co-EPD

Co-EPD of elements with different particle size can be very complex and interesting. Boccaccini et al. reported a TiO₂ coated carbon nanotubes (CNTs) obtained by co-EPD and they believe that the different electric surface charge on each object is the key to make the smaller sized TiO₂ nano-particles attaching on the CNTs [25]. In this work, silicon nano-particle coated galinstan droplets were initially observed on occasion (*Fig. 5.2a*). Then Ni²⁺ charged galinstan is mixed with self negatively charged silicon nano-particles right before co-EPD. It is believed that some of the self negatively charged Si nano-particles were attracted to the surface of Ni²⁺ charged galinstan particles by the electrostatic force between the opposite charges. A graphic explanation of this mechanism is showed in *Fig.5.2c*. By doing this, a silicon nano-particle coated galinstan thin film is obtained (*Fig. 5.2b*). Further experiments and theoretical analyses are needed to confirm and better understand the mechanism of core-shell silicon – galinstan structure by co-EPD.

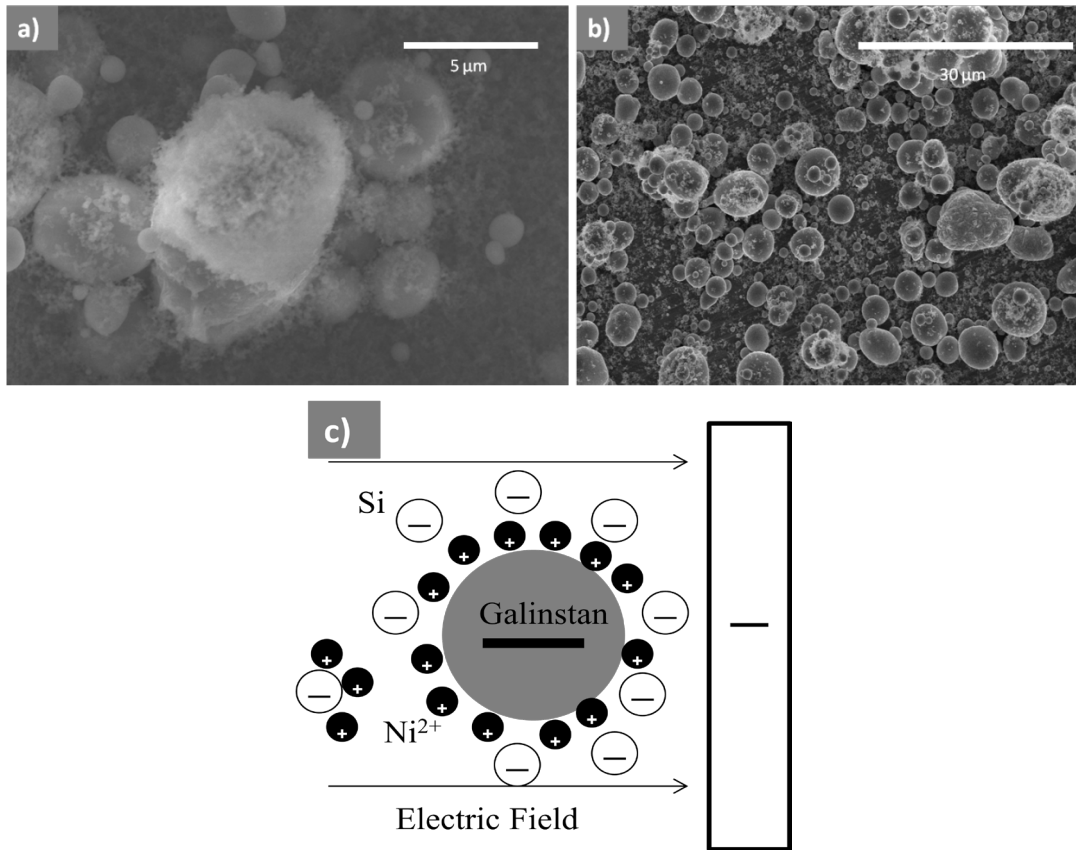


Fig.5.2 a) the Si-galinstan core-shell structure which may be ideal for lithium-ion insertion; b) galinstan droplets with slight silicon nano particle coating; c) Schematic view of core-shell formation mechanism in co-EPD.

5.3. Half-cell test performance

The initial result of the LIB half-cell testing indicates that the nano-silicon and galinstan electrode has a relevantly higher capacity (1500 mAh/g) at 1st discharge than that of micron-silicon, yet the problem of fast capacity fading still remains.

Conductivity of the electrode may also be an issue because the 1st discharge capacities of the samples are much lower than the theoretical capacity (4200 mAh/g) of Si based negative electrode. Conductive additive such like carbon nanotubes (CNTs) can be introduced to improve the conductivity of the film. Other than that, the possible irreversible alloy formed by lithium and galinstan will also cause the fast fading. *Fig.5.3* shows the differential capacity (dQ/dE) and potential curve of galinstan and lithium system. The 1st discharge (Li⁺ insertion to galinstan) is a multiple-stage discharge, and each peak of the curve represents a fast electron transferring, indicating a reaction or a material phase change is happening within the system. Compare to the 1st discharge curve, the 1st charge (Li⁺ extraction) curve has less peaks. The asymmetric charge/discharge curves imply that galinstan contains irreversible alloy after lithium ion insertion. This issue can also be

noticed by comparing the 2nd discharge (2nd Li⁺ insertion) curve to the 1st discharge curve. The peaks in 2nd discharge curve are much less and smaller than that of the 1st discharge, which means less material are available for Li⁺ insertion, consequently, a capacity fading is observed.

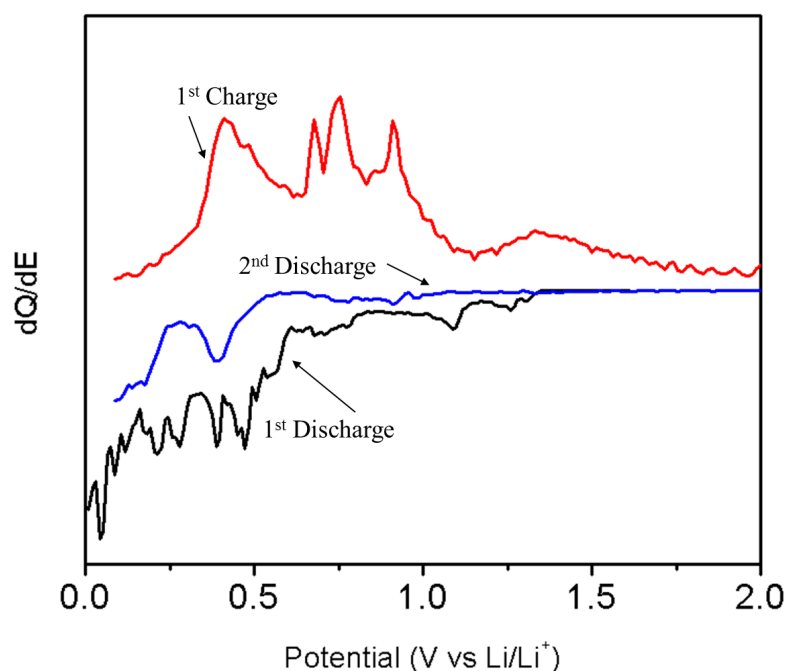


Fig.5.3 *Asymmetric differential capacity (dQ/dE) vs potential curves of galinstan-lithium charge/discharge*

The irreversible compounds may be formed between the lithium and the individual metals in galinstan (Gallium, Indium and Tin), and it can also be the impurities in the film, such like oxidation layer of galinstan and Ni holding layer.

5.4. Issues and challenges – Ga-Li system

Although the negative electrode fabrication was successful and the initial test results were positive, capacity fading is still an issue for this Si - galinstan system. The potential irreversible gallium-lithium alloy, Li_xGa_y , has been reported by many people and it is believed that the possible formation of these alloy will weaken the cell performance as most of these compounds are solid [26, 27]. However, recently Liang et al. demonstrated the reversible liquid-solid-liquid transformation of gallium nano-droplets during the charge/discharge cycling by using *in situ* transmission electron microscopy (TEM) [28]. The lithiation of gallium is a multiple stage process, where the first phase change of gallium to Li_2Ga_7 is happened at the potential of ~ 0.6 V vs. Li/Li^+ [29]. This potential is higher than the first silicon-lithium reaction potential (~ 0.2 V vs. Li/Li^+), which implies that gallium will react to Li^+ first during lithiation and becomes solid. **Fig.5.4** shows the schematic comparison between gallium-lithium reaction and silicon-lithium reaction. Although the $\text{Ga-Li}_2\text{Ga-Ga}$ transformation will have a 600 mAh/g specific capacity and its phase change seems to be reversible, the dynamic gallium-lithium-silicon interaction remains unknown. Furthermore, while the galinstan-lithium interaction may behave similarly to the

gallium-lithium interaction since galinstan is made of 68w% gallium, no experimental data were found to support such hypothesis.

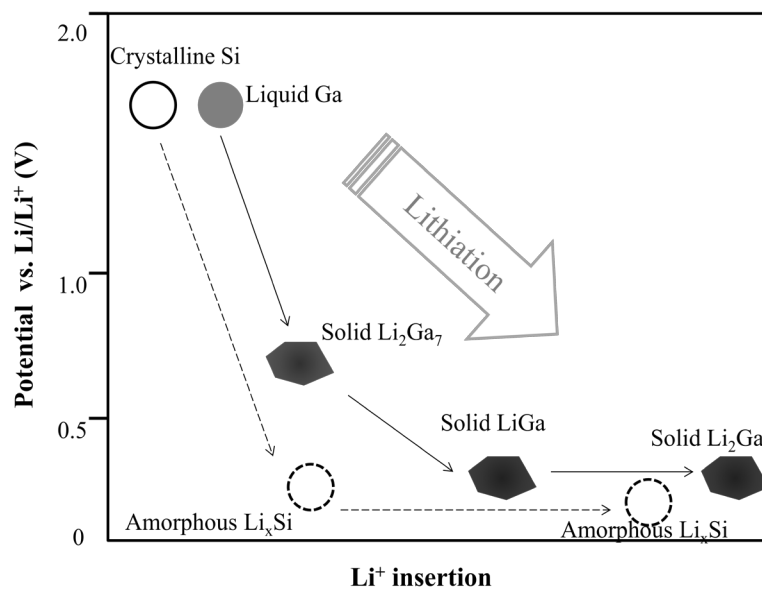


Fig5.4. Schematic lithiation comparison of Si and Ga

6. Future Work

6.1. Application of liquid metal thin film by EPD - CIGS solar cell

$\text{CuIn}_{(1-x)}\text{Ga}_{(x)}\text{Se}_2$ (CIGS) is an active material for thin film solar cell which can have a high efficiency of over 20%. Typical synthesis method of CIGS includes Physical Vapor Deposition (PVD), Chemical Bath Deposition (CBD) and other low cost methods such like pasting and ball milling [30-33]. PVD can have an accurate control of the composition by monitoring the vapor supplier of each element, but the cost is the highest of all. CBD, typically electroplating, may be another good choice as it is relevantly cheaper than PVD process by electroplating the salt of gallium, copper and indium followed by an annealing process in selenium environment. However the efficiency of electroplated CIGS is usually low because the composition of the product is difficult to control as the reduction potential of the elements in the solution are quite different [14].

Co-EPD process may be a possible solution to the low cost, fast fabrication of CIGS thin film. EPD of gallium was reported in this work

with its high deposition rate compare to electroplating verified. Using co-EPD method for the deposition of gallium, copper, indium and selenium particles can potentially be an efficient way of CIGS synthesis without vacuum process and reduction potential issue.

7. Conclusion

Synthesizing and testing of silicon and galinstan co-deposited film as lithium-ion battery negative electrode was successfully performed. Despite the fast fading issue, an initial capacity of 1500 mAh/g was observed from half-cell test. At the same time, EPD method was first time reported to be used on liquid metal thin film deposition, which may open the opportunity for other applications such like CIGS thin film solar cell fabrication.

Reference

- [1] M. Mohri, N. Yanagisawa, Y. Tajima, H. Tanaka, T. Mitate, S. Nakajima, M. Yoshida, Y. Yoshimoto, T. Suzuki, and H. Wada, "Rechargeable lithium battery based on pyrolytic carbon as a negative electrode," *Journal of Power Sources*, vol. 26, pp. 545-551, 1989.
- [2] Z. Yang, H.-Q. Wu, and B. Simard, "Charge–discharge characteristics of raw acid-oxidized carbon nanotubes," *Electrochemistry Communications*, vol. 4, pp. 574-578, 2002.
- [3] B. A. Boukamp, G. C. Lesh, and R. A. Huggins, "All - Solid Lithium Electrodes with Mixed - Conductor Matrix," *Journal of The Electrochemical Society*, vol. 128, pp. 725-729, April 1, 1981 1981.
- [4] J. H. Ryu, J. W. Kim, Y.-E. Sung, and S. M. Oh, "Failure Modes of Silicon Powder Negative Electrode in Lithium Secondary Batteries," *Electrochemical and Solid-State Letters*, vol. 7, pp. A306-A309, 2004.
- [5] K. E. Aifantis and J. P. Dempsey, "Stable crack growth in nanostructured Li-batteries," *Journal of Power Sources*, vol. 143, pp. 203-211, Apr 27 2005.
- [6] R. Lv, J. Yang, J. Wang, and Y. NuLi, "Electrodeposited porous-microspheres Li–Si films as negative electrodes in lithium-ion batteries," *Journal of Power Sources*, vol. 196, pp. 3868-3873, 2011.
- [7] M.-H. Park, M. G. Kim, J. Joo, K. Kim, J. Kim, S. Ahn, Y. Cui, and J. Cho, "Silicon Nanotube Battery Anodes," *Nano Letters*, vol. 9, pp. 3844-3847, 2009/11/11 2009.
- [8] C. K. Chan, H. Peng, G. Liu, K. McIlwrath, X. F. Zhang, R. A. Huggins, and Y. Cui, "High-performance lithium battery anodes using silicon nanowires," *Nat Nano*, vol. 3, pp. 31-35, 2008.

- [9] L. Ji, H. Zheng, A. Ismach, Z. Tan, S. Xun, E. Lin, V. Battaglia, V. Srinivasan, and Y. Zhang, "Graphene/Si multilayer structure anodes for advanced half and full lithium-ion cells," *Nano Energy*, vol. 1, pp. 164-171, 2012.
- [10] Y.-Z. Chiou, Y.-K. Su, S.-J. Chang, and C.-H. Chen. (2003, GaN metal-semiconductor interface and its applications in GaN and InGaN metal-semiconductor-metal photodetectors. *IEE Proceedings - Optoelectronics* 150(2), 115-118.
- [11] R. Tayrani and R. W. Glew. (1983, Ultrafast GaAs microwave PIN diode. *Electronics Letters* 19(13), 479-480.
- [12] Y. Liu and D. Kong. (2012, Synthesis and characteristics of Cu(In,Ga)Se₂ thin films from nanoparticles by solvothermal method and selenisation process. *Micro & Nano Letters* 7(11), 1112-1116.
- [13] A. B. C. Ashby, *Introduction to GaAs devices*, 2005.
- [14] V. S. Saji, I.-H. Choi, and C.-W. Lee, "Progress in electrodeposited absorber layer for CuIn(1-x)Ga_xSe₂ (CIGS) solar cells," *Solar Energy*, vol. 85, pp. 2666-2678, 2011.
- [15] L. Besra and M. Liu, "A review on fundamentals and applications of electrophoretic deposition (EPD)," *Progress in Materials Science*, vol. 52, pp. 1-61, 2007.
- [16] J. W. S. A. B. M. Basol, "Gallium Electroplating Methods and Electrolytes Employing Mixed Solvents," US 7,951,280 B2, 2011.
- [17] Y. S. Joung and C. R. Buie, "Electrophoretic Deposition of Unstable Colloidal Suspensions for Superhydrophobic Surfaces," *Langmuir*, vol. 27, pp. 4156-4163, 2011/04/05 2011.
- [18] C. L. Yaws, *Chemical Properties Handbook*: McGraw-Hill, 1999.
- [19] M. F. Meléndrez, G. Cárdenas, and J. Arbiol, "Synthesis and characterization of gallium colloidal nanoparticles," *Journal of Colloid and Interface Science*, vol. 346, pp. 279-287, 2010.
- [20] D. C. Company, *Calcium Chloride Handbook*: Dow Chemical Company, 1966.

- [21] S. Santhanagopalan, F. Teng, and D. D. Meng, "High-Voltage Electrophoretic Deposition for Vertically Aligned Forests of One-Dimensional Nanoparticles," *Langmuir*, vol. 27, pp. 561-569, 2011/01/18 2010.
- [22] J. B. Talbot, E. Sluzky, and S. K. Kurinec, "Electrophoretic deposition of monochrome and color phosphor screens for information displays," *Journal of Materials Science*, vol. 39, pp. 771-778, 2004.
- [23] H. C. Hamaker, "Formation of a deposit by electrophoresis," *Transactions of the Faraday Society*, vol. 35, pp. 279-287, 1940.
- [24] M. Steichen, M. Thomassey, S. Siebentritt, and P. J. Dale, "Controlled electrodeposition of Cu-Ga from a deep eutectic solvent for low cost fabrication of CuGaSe₂ thin film solar cells," *Physical Chemistry Chemical Physics*, vol. 13, pp. 4292-4302, 2011.
- [25] A. R. Boccaccini, J. Cho, J. A. Roether, B. J. C. Thomas, E. Jane Minay, and M. S. P. Shaffer, "Electrophoretic deposition of carbon nanotubes," *Carbon*, vol. 44, pp. 3149-3160, 2006.
- [26] J. Hafner and W. Jank, "Structural and electronic properties of crystalline and molten Zintl phases: The Li-Ga system," *Physical Review B*, vol. 44, pp. 11662-11676, 1991.
- [27] J. Saint, M. Morcrette, D. Larcher, and J. M. Tarascon, "Exploring the Li-Ga room temperature phase diagram and the electrochemical performances of the Li_xGa alloys vs. Li," *Solid State Ionics*, vol. 176, pp. 189-197, 2005.
- [28] W. Liang, L. Hong, H. Yang, F. Fan, Y. Liu, H. Li, J. Li, J. Y. Huang, L.-Q. Chen, T. Zhu, and S. Zhang, "Nanovoid Formation and Annihilation in Gallium Nanodroplets under Lithiation-Delithiation Cycling," *Nano Letters*, vol. 13, pp. 5212-5217, 2013/11/13 2013.
- [29] R. D. Deshpande, J. Li, Y.-T. Cheng, and M. W. Verbrugge, "Liquid Metal Alloys as Self-Healing Negative Electrodes for

- Lithium Ion Batteries," *Journal of The Electrochemical Society*, vol. 158, pp. A845-A849, August 1, 2011 2011.
- [30] P. Jackson, D. Hariskos, E. Lotter, S. Paetel, R. Wuerz, R. Menner, W. Wischmann, and M. Powalla, "New world record efficiency for Cu(In,Ga)Se₂ thin-film solar cells beyond 20%," *Progress in Photovoltaics: Research and Applications*, vol. 19, pp. 894-897, 2011.
- [31] D. Xia, J. Li, M. Xu, and X. Zhao, "Electrodeposited and selenized CIGS thin films for solar cells," *Journal of Non-Crystalline Solids*, vol. 354, pp. 1447-1450, 2008.
- [32] M. Kaelin, D. Rudmann, F. Kurdesau, H. Zogg, T. Meyer, and A. N. Tiwari, "Low-cost CIGS solar cells by paste coating and selenization," *Thin Solid Films*, vol. 480–481, pp. 486-490, 2005.
- [33] C. P. Liu and C. L. Chuang, "Fabrication of CIGS nanoparticle-ink using ball milling technology for applied in CIGS thin films solar cell," *Powder Technology*, vol. 229, pp. 78-83, 2012.